

Article

Off-Axis Vortex Beam Propagation through Classical Optical System in Terms of Kummer Confluent Hypergeometric Function

Ireneusz Augustyniak ¹, Weronika Lamperska ^{2,*} , Jan Masajada ² , Łukasz Płociniczak ¹  and Agnieszka Popiołek-Masajada ² 

¹ Department of Applied Mathematics, Faculty of Pure and Applied Mathematics, Wrocław University of Science and Technology, Wybrzeże Wyspiańskiego 27, 50-370 Wrocław, Poland; ireneusz.augustyniak@pwr.edu.pl (I.A.); lukasz.plociniczak@pwr.edu.pl (Ł.P.)

² Department of Optics and Photonics, Faculty of Fundamental Problems of Technology, Wrocław University of Science and Technology, Wybrzeże Wyspiańskiego 27, 50-370 Wrocław, Poland; jan.masajada@pwr.edu.pl (J.M.); agnieszka.masajada@pwr.edu.pl (A.P.-M.)

* Correspondence: weronika.lamperska@pwr.edu.pl

Received: 16 July 2020; Accepted: 14 August 2020; Published: 15 August 2020



Abstract: The analytical solution for the propagation of the laser beam with optical vortex through the system of lenses is presented. The optical vortex is introduced into the laser beam (described as Gaussian beam) by spiral phase plate. The solution is general as it holds for the optical vortex of any integer topological charge, the off-axis position of the spiral phase plate and any number of lenses. Some intriguing conclusions are discussed. The higher order vortices are unstable and split under small phase or amplitude disturbance. Nevertheless, we have shown that off-axis higher order vortices are stable during the propagation through the set of lenses described in paraxial approximation, which is untypical behavior. The vortex trajectory registered at image plane due to spiral phase plate shift behaves like a rigid body. We have introduced a new factor which in our beam plays the same role as Gouy phase in pure Gaussian beam.

Keywords: optical vortex; angular momentum; optical microscopy; singular optics; hypergeometric function; Kummer function

1. Introduction

The question of generation and propagation of light fields containing optical vortices [1–3] is getting attention in many fields of modern optical science nowadays. The fundamental case of such a field is vortex beam—the well-defined, single beam (as, for example, LG beam [4,5]), carrying the optical vortex of any order. Many different problems concerning the generation and propagation of the vortex beam have been considered in the literature so far. Some of them consider optical fields containing the lattice of vortices generated, for example, by three or more plane or spherical waves interference [6–9]; or so called composed vortices, i.e., vortices which are generated by two or more overlapping beams [10–16].

The study on single vortex beam propagation has started with the most basic problem, that is propagation of the fundamental vortex beam in a free space [17–19]. Next, the problem of vortex beam generation by the simple optical element revealing circular symmetry was reported [20,21]. Here, the most important part for our study are papers devoted to Gaussian beam propagation through the spiral phase plate (SPP) [22–28]. SPP is now one of the most common ways of introducing optical vortex into the laser beam. In more advanced approaches the propagation of vortex beam with broken symmetry or through the system with broken symmetry (like, for example, diffraction by

half-plane [29,30] or a phase step [31,32]) was studied. Most of these asymmetrical cases were studied combining numerical and/or strongly approximated analytical method, especially in case of higher order vortices [33–41]. Another highly asymmetrical problem is a vortex beam propagation through the turbid media (e.g., atmosphere) [42–44] or vortex generation with polarization optics such as q-plates [45].

In the paper [34] the analysis of the Gaussian beam propagation through the off-axis SPP in Fraunhofer approximation is studied. Authors have focused their attention on the vortex point displacement measured by inspecting the asymmetry in intensity distribution at the far field. In the present paper we analyze asymmetrical optical system with Fresnel diffraction theory, which is more general than Fraunhofer one. The analysis of the off-axis high-order vortices is a difficult task. The integrals become highly complicated and some typical tricks often used in the calculations cannot be applied. The good example is stationary phase method [46], which cannot be used since the phase changes very fast in the vicinity of the vortex point. That is the reason why there are only few publications regarding the exact solutions of asymmetric higher order vortex propagation. In paper [47] the elliptic vortex beam propagation is studied. The paper [48] describes the generation of the higher order vortex beam by discretizing spiral phase plate. In paper [49] the generation of vortex beam through fractional spiral phase plate is studied. In papers [50,51] the propagation through off-axis hologram generating the optical vortices is analyzed, also including the effects of misalignment.

In papers [52,53] we have provided a solution for asymmetrical vortex propagation in optical vortex scanning microscope (OVSM) presented schematically in Figure 1. In this paper we propose more general solution in terms of Kummer confluent hypergeometric function which can be used for a system of arbitrary number of lenses. This function has been already used for defining the new beam family produced by the four-component system (of circular symmetry)–logarithmic axicon, SPP, amplitude power function and Gaussian function [54]. Furthermore, the asymmetrical Gaussian vortex beam generated by the off-axis SPP or fork-like hologram has been studied in paper [55] but in a different way–no propagation through the classical optical system was included. The context of photon entanglement via angular momentum [56,57] mentioned in the paper [55] shows that the analysis of the off-axis Gaussian vortices is important to this very hot topics in modern physics.

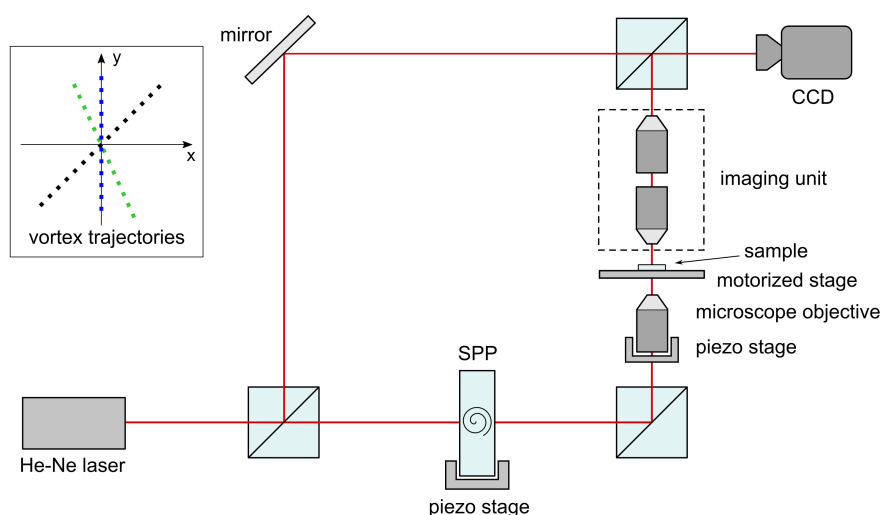


Figure 1. The scheme of optical vortex scanning microscope (OVSM). In the inset the registered three vortex trajectories are shown. The vortex trajectories are subsequent positions of vortex point (vortex point is a point where the phase is singular) at sample plane while moving the SPP perpendicularly to the optical beam. The three trajectories were measured at three slightly different positions of focusing objective. This objective was moved toward the sample.

In this paper the optical system shown schematically in Figure 2 is studied. The system represents the object arm of the OVSM shown in Figure 1 (in experiment, the reference arm is necessary for reconstructing both amplitude and phase of the object beam. Obviously, in analytical and numerical calculations we do not need it). The system is divided into blocks. Each block consists of one or more elements and is represented by its transmittance function (in case of single element) or the product of the transmittance functions (when there are two or more elements in the given block). In our first approach [52] the OVSM was reduced to a single block consisting of three elements, i.e., incident Gaussian beam, SPP and focusing lens considered as a single thin element. The image was calculated at the sample plane (noted as sample in Figure 1). It should be noticed that the SPP can be moved perpendicularly to the optical axis, which breaks the system symmetry. As a result, the vortex point moves inside the focused beam, but the range of this movement is highly reduced due to focusing lens. The inset in Figure 1 shows the exemplary vortex trajectories as registered in our experimental system. In this way the sample can be scanned with the vortex point (i.e., point where the phase is singular). This technique is named the Internal Scanning Method (ISM) [37,39,52,53,58,59]. In the paper [53] the system built of three blocks was analyzed. The first block consisted of incident Gaussian beam, SPP and focusing lens, the second was just the sample plane, and the third contained a single imaging lens. Here, we extend the analysis to the fully expanded system shown in Figure 2b.

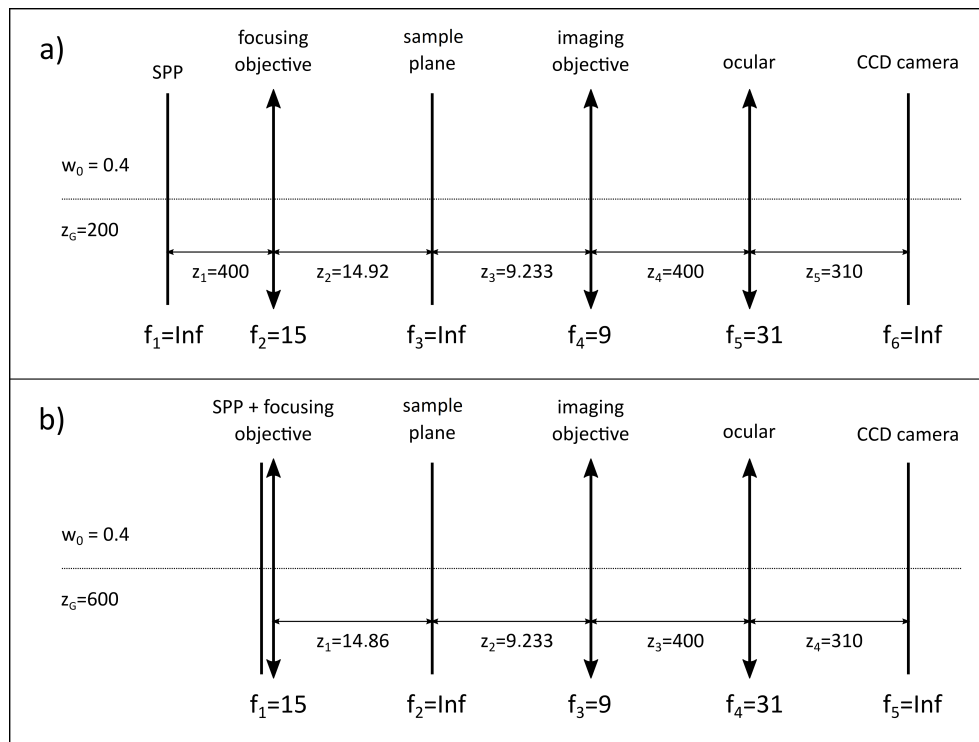


Figure 2. Two versions of the OVSM scheme; (a) the SPP is separated from the focusing lens; (b) the SPP and focusing objective work together as a single thin element. In both cases the imaging objective and the ocular form the image of the sample plane on CCD camera. Units: [mm].

Our analysis was performed within the frame of scalar diffraction theory in Fresnel approximation [60]. The Fresnel diffraction integral for the first block shown in Figure 2b has a form

$$\begin{aligned}
 u(x_1, y_1) = & \frac{-i}{\lambda z_1} \iint_{\mathbb{R}^2} T_v(x, y) u_G(x - x_c, y) T_f(x - x_c, y) \\
 & \times e^{\frac{ik}{2z_1}(x_1^2 + y_1^2)} e^{\frac{ik}{2z_1}[(x - x_c)^2 + y^2]} e^{-\frac{ik}{z_1}[(x - x_c)x_1 + yy_1]} dx dy
 \end{aligned}
 \tag{1}$$

where k is a wave number, λ is a wavelength, T_v is a transmittance function of the SPP, u_G is an incident Gaussian beam, T_f is a transmittance function of the focusing lens.

$$T_v = e^{im\phi} \tag{2a}$$

$$u_G = e^{-\left(\frac{1}{w^2(z)} + \frac{ik}{2R(z)}\right)[(x-x_c)^2 + y^2]} \tag{2b}$$

$$T_f = e^{-\frac{ik}{2f_1}[(x-x_c)^2 + y^2]} \tag{2c}$$

$$w^2(z) = w_0^2 \left(1 + \left(\frac{\lambda z}{\pi w_0^2} \right)^2 \right) \tag{2d}$$

$$R(z) = z \left(1 + \left(\frac{\pi w_0^2}{\lambda z} \right)^2 \right) \tag{2e}$$

m is a topological charge of the optical vortex; it is an integer—positive or negative, w_0 is a beam waist (of the Gaussian beam), f_1 is a focal length of the focusing lens.

Instead of moving the SPP off the optical axis by the distance x_c we moved the rest of the system (including the screen) by the same x_c , which simplified further calculations. As was shown in [52] the integral Equation (1) had a solution

$$u_1(x_1, y_1) = \Xi_1 K(A^{(1)}, B_x^{(1)}, B_y^{(1)}, C^{(1)}) \tag{3}$$

where

$$\Xi_1 = \frac{e^{ikz_1}}{i\lambda z_1} e^{iknd_1} U_0 \frac{w_0}{w(z)} e^{i[\arctan(\frac{z}{R}) - kz + \omega t]} \tag{4a}$$

$$A^{(1)} = \alpha + i\beta \tag{4b}$$

$$B_x^{(1)} = -2x_c(\alpha + i\beta) - \frac{ikx_1}{z_1} \tag{4c}$$

$$B_y^{(1)} = -\frac{iky_1}{z_1} \tag{4d}$$

$$C^{(1)} = x_c^2(\alpha + i\beta) + \frac{ik}{2z_1}(x_1^2 + y_1^2) + \frac{ikx_c x_1}{z_1} \tag{4e}$$

The parameters α and β are

$$\alpha = -\frac{1}{w^2(z)} \tag{4f}$$

$$\beta = -\frac{k}{2} \left(\frac{1}{R(z)} + \frac{1}{f_1} - \frac{1}{z_1} \right) \tag{4g}$$

The main part of this solution is function Kappa K .

$$K(A, B_x, B_y, C) = -\frac{\sqrt{\pi} \cdot e^C}{2A} \times \begin{cases} \sqrt{\pi} \sum_{n=0}^{\infty} \frac{1}{n!(2\sqrt{-A})^{2n+1}} \sum_{j=0}^{2n+1} \binom{2n+1}{j} B_x^j B_y^{2n+1-j} \sum_{l=0}^m \binom{m}{l} i^l J_{m+j-l, 2n+1-j+l}; & \text{for } m \text{ odd} \\ \sum_{n=0}^{\infty} \frac{2^{n+1}}{(2n+1)!!(2\sqrt{-A})^{2n+2}} \sum_{j=0}^{2n+2} \binom{2n+2}{j} B_x^j B_y^{2n+2-j} \sum_{l=0}^m \binom{m}{l} i^l J_{m+j-l, 2n+2-j+l}; & \text{for } m \text{ even} \end{cases} \tag{5a}$$

where

$$J_{\delta, \eta} = \int_0^{2\pi} (\cos \varphi)^\delta (\sin \varphi)^\eta d\varphi \tag{5b}$$

We have obtained an interesting result showing that a system having more blocks (with lenses or just planes) can still be described by Kappa function, but with different coefficients $\Xi_q, A^{(q)}, B_x^{(q)}, B_y^{(q)}, C^{(q)}$. The number of blocks in the system is indicated by superscript (q) as it has been already done in Equations (3) and (4). In paper [53] we calculated explicitly the coefficients $\Xi_q, A^{(q)}, B_x^{(q)}, B_y^{(q)}, C^{(q)}$ up to $q = 3$, and postulated that it can be done for any (q). In this paper we derived a recurrence formula for the coefficient for any number of blocks (any (q)), which is actually a formal proof of our previous claim.

The function Kappa was denoted previously as G [52,53]. Since that time we have improved and generalized our solution. Now the function G is rewritten in more useful form. In order not to confuse both versions, we denote the present version by capital Kappa K .

As it was shown in papers [52,53], close to the vortex axis the $n = 0$ term is sufficient to evaluate the vortex beam. Figure 3 illustrates this fact, but now it is plotted for the four-block system shown in Figure 2b. This is a useful result for us, as we analyze the OVSM images at the central part of the beam, where the $n = 0$ approximation well represents phase and amplitude distribution of our beam.

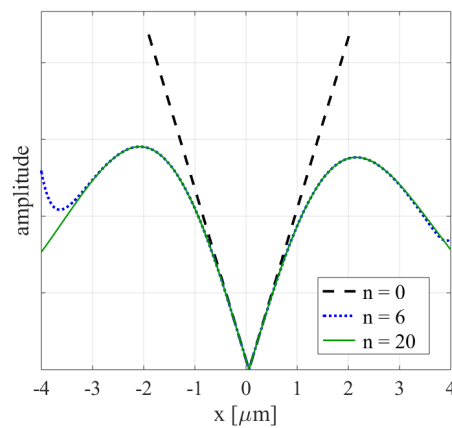


Figure 3. The amplitude distribution of the off-axis vortex beam ($m = 1, x_c = 0.02$ mm) for the system shown in Figure 2b in case of $n = 0, n = 6$ and $n = 20$.

Our goal was to represent the entire object arm of the OVSM as presented in Figure 2a. Now the SPP can be separated from the focusing lens which means that focal length for the first block (i.e., SPP block) is $f_1 = \infty$. Next there is a focusing lens with focal length $f_2 = 15$ mm followed by the sample plane for which the focal length is also infinite $f_3 = \infty$. The third block is the imaging lens with focal length $f_4 = 9$ mm and the last one is the ocular lens with focal length $f_5 = 31$ mm, after which we have observation plane (screen). Unfortunately, for the reasons given later in the manuscript the full system could not be analyzed with Kappa function. The SPP cannot be separated from the focusing lens. Therefore, we have to switch to the system shown in Figure 2b. In this paper we will analyze this system showing the efficiency of our formulas. As can be noticed from Figure 2b, in our model a sample plane is treated as a separate block. In this way we are able to enhance our calculations in order to analyze the influence of a simple phase object on the vortex beam. Thus, the system shown in Figure 2b prepares us for this next step.

Certainly, all the blocks may have different focal lengths and positions than the ones shown in Figure 2 and the Kappa function will still work. However, the important thing is that the first element must be the block containing the SPP, focusing lens and Gaussian beam. Thus, we can model a wide range of classical optical systems with the incident vortex beam generated by the SPP. The analytical modelling means that the analyzed optical system is highly simplified, but on the other hand supports a general insight which is still valuable in solving practical problems. Our work can be also considered as solving the diffraction problem in the paraxial approximation for the specific

optical system. However, the expression “analytical modelling” is more preferable since it emphasizes our focus on practical aspects, i.e., development of the OVSM system for which our former results have been already used [58,59].

We realize that after this long introduction the Reader may be lost concerning the question of what is new in the presented paper. To avoid confusion the new aspects of this paper are summarized in brief. At first, we extend our previous formulas from three to any number of elements in the optical system. Then, the formulas are written in closed form using the special functions. This step speeds up all calculations and allows proving the hypothesis that the higher order vortices propagate in a stable way in our system, which is a surprising result. We also study in detail the role of coefficient A which plays a role similar to the Gouy phase in case of Gaussian beam. Finally, we show that vortex trajectory behaves like a rigid body while being rotated due to observation plane shift.

The present paper is organized as follows. In Section 2 the extension of our formulas as well as their closed form for the system consisting of any number of lenses is discussed. In Section 3 we discussed the role of coefficient A . In Section 4 we show the efficiency of our formulas by discussing the effect of vortex trajectory rotation. Section 5 and Section 6 discuss and conclude the paper.

2. Analytical Part

In this part our previous results will be extended. In order to build more relevant model of the OVSM we have derived the explicit formula for coefficients $\Xi_q, A^{(q)}, B_x^{(q)}, B_y^{(q)}, C^{(q)}$ up to $q = 4$, just to analyze the OVSM system shown in Figure 2b.

$$\Xi_4 = \frac{e^{ik(z_1+z_2+z_3+z_4)}}{\lambda^4 z_1 z_2 z_3 z_4} e^{ikn(d_1+d_2+d_3+d_4)} U_0 \frac{w_0}{w(z)} e^{i[\arctan(\frac{z}{z_R})-kz+\omega t]} \tag{6a}$$

$$A^{(4)} = \alpha + i\beta - \frac{ik}{2z_1^2 \gamma_2} - \frac{ik}{2z_1^2 z_2^2 \gamma_2^2 \gamma_3} - \frac{ik}{2z_1^2 z_2^2 z_3^2 \gamma_2^2 \gamma_3^2 \gamma_4} \tag{6b}$$

$$B_x^{(4)} = -2x_c(\alpha + i\beta) + \frac{ikx_c}{z_1^2 \gamma_2} + \frac{ikx_c}{z_1^2 z_2^2 \gamma_2^2 \gamma_3} - \frac{ik}{z_1 z_2 z_3 \gamma_2 \gamma_3 \gamma_4} \left(\frac{x_4}{z_4} - \frac{x_c}{z_1 z_2 z_3 \gamma_2 \gamma_3} \right) \tag{6c}$$

$$B_y^{(4)} = -\frac{iky_4}{z_1 z_2 z_3 z_4 \gamma_2 \gamma_3 \gamma_4} \tag{6d}$$

$$C^{(4)} = x_c^2(\alpha + i\beta) + \frac{ik}{2z_4} (x_4^2 + y_4^2) - \frac{ikx_c^2}{2z_1^2 \gamma_2} - \frac{ikx_c^2}{2z_1^2 z_2^2 \gamma_2^2 \gamma_3} - \frac{ik}{2\gamma_4} \left[\left(\frac{x_4}{z_4} - \frac{x_c}{z_1 z_2 z_3 \gamma_2 \gamma_3} \right)^2 + \left(\frac{y_4}{z_4} \right)^2 \right] \tag{6e}$$

$$\gamma_4 = \frac{1}{z_3} + \frac{1}{z_4} - \frac{1}{f_4} - \frac{1}{z_3^2 \gamma_3} \tag{6f}$$

$$\gamma_3 = \frac{1}{z_2} + \frac{1}{z_3} - \frac{1}{f_3} - \frac{1}{z_2^2 \gamma_2} \tag{6g}$$

$$\gamma_2 = \frac{1}{z_1} + \frac{1}{z_2} - \frac{1}{f_2} \tag{6h}$$

where the meaning of z_4 and f_4 can be read from Figure 2), d_1, \dots, d_4 are lens thicknesses. In case of a simple plane we put $d = 0$.

Following this path a general iterative formulas for coefficient of any (q) index can be derived. The formulas have a form

$$u_j(x_j, y_j) = \xi_j \iint_{\mathbb{R}^2} u_{j-1}(x_{j-1}, y_{j-1}) e^{\frac{ik}{2z_j}(x_j^2 + y_j^2)} e^{\frac{ik}{2z_j}(x_{j-1}^2 + y_{j-1}^2)} e^{-\frac{ik}{2f_j}(x_{j-1}^2 + y_{j-1}^2)} \times e^{-\frac{ik}{z_j}(x_{j-1}x_j + y_{j-1}y_j)} dx_{j-1} dy_{j-1} \tag{7a}$$

$$u_j(x_j, y_j) = \Xi_j \left(\frac{2i\pi}{k} \right)^{j-1} \prod_{s=1}^j \frac{1}{\gamma_s} \cdot K(A^{(j)}, B_x^{(j)}, B_y^{(j)}, C^{(j)}) \tag{7b}$$

$$A^{(j)} = \alpha + i\beta - \frac{ik}{2} \sum_{p=1}^{j-1} \prod_{s=1}^p \frac{1}{z_s^2 \gamma_s^2 \gamma_j} \tag{8a}$$

$$B_x^{(j)} = -2x_c(\alpha + i\beta) + ikx_c \sum_{p=1}^{j-1} \prod_{s=1}^p \frac{1}{z_s^2 \gamma_s^2 \gamma_j} - \frac{ikx_j}{\prod_{s=1}^j z_s \gamma_s} \tag{8b}$$

$$B_y^{(j)} = -\frac{iky_j}{\prod_{s=1}^j z_s \gamma_s} \tag{8c}$$

$$C^{(j)} = x_c^2(\alpha + i\beta) + \frac{ik}{2z_j}(x_j^2 + y_j^2) - \frac{ikx_c^2}{2} \sum_{p=1}^{j-1} \prod_{s=1}^p \frac{1}{z_s^2 \gamma_s^2 \gamma_j} + \frac{ikx_c x_j}{2 \prod_{s=1}^j z_s \gamma_s} - \frac{ik}{2z_j^2 \gamma_j}(x_j^2 + y_j^2) \tag{8d}$$

$$\gamma_j = \frac{1}{z_{j-1}} + \frac{1}{z_j} - \frac{1}{f_j} - \frac{1}{z_{j-1}^2 \gamma_{j-1}} \tag{8e}$$

$$\Xi_j = \frac{e^{ik \sum_{s=1}^j z_s}}{ij \lambda^j \prod_{s=1}^j z_s} e^{ikn \sum_{s=1}^j d_s} U_0 \frac{w_0}{w(z)} e^{i[\arctan(\frac{z}{R}) - kz + \omega t]} \tag{8f}$$

$$\gamma_0 = \gamma_1 = 1, j \in \mathbb{N}_+ \tag{8g}$$

The derivation of the above is presented in Appendix A.

The sums in Kappa function are convergent provided that a series of conditions are hold

$$\frac{1}{z_j} > \frac{1}{f_j} + \frac{1}{\gamma_{j-1}} - \frac{1}{z_{j-1}}; j \leq q \tag{9}$$

Very similar formulas can be derived for negative vortex charge. In that case we can use the same Kappa function but with some multiplying expression and B_y coefficient multiplied by -1 .

$$u_{j-}(x_j, y_j) = -e^{-i2\pi m} \Xi_j K(A^{(j)}, B_x^{(j)}, -B_y^{(j)}, C^{(j)}) \tag{10}$$

The derivation of this formula is presented in Appendix B.

We have also derived a closed formula, but with a special function, which is given below. The derivation is discussed in the Appendix C.

$$u_q(x_q, y_q) = -\Xi_q \frac{\pi\sqrt{\pi}e^{C(q)}}{2^m\sqrt{-A(q)}} \frac{1}{\left(\frac{m-1}{2}\right)!} \left(\frac{B_x^{(q)}}{2\sqrt{-A(q)}} + i\frac{B_y^{(q)}}{2\sqrt{-A(q)}}\right)^m \times {}_1F_1\left(1 + \frac{m}{2}, 1 + m, \left(\frac{B_x^{(q)}}{2\sqrt{-A(q)}}\right)^2 + \left(\frac{B_y^{(q)}}{2\sqrt{-A(q)}}\right)^2\right); \text{ for } m \text{ odd} \tag{11a}$$

$$u_q(x_q, y_q) = \Xi_q \frac{\pi e^{C(q)}}{2^{\frac{m}{2}}\sqrt{-A(q)}} \frac{1}{(m-1)!!} \left(\frac{B_x^{(q)}}{2\sqrt{-A(q)}} + i\frac{B_y^{(q)}}{2\sqrt{-A(q)}}\right)^m \times {}_1F_1\left(1 + \frac{m}{2}, 1 + m, \left(\frac{B_x^{(q)}}{2\sqrt{-A(q)}}\right)^2 + \left(\frac{B_y^{(q)}}{2\sqrt{-A(q)}}\right)^2\right); \text{ for } m \text{ even} \tag{11b}$$

where ${}_1F_1$ is the Kummer confluent hypergeometric function [61]. The calculations using closed formula are much faster, but as we will show both formulas Equations (3) and (11) are helpful in understanding the vortex beam propagation through our system.

The sum of two B coefficients in Equation (8b,c) is a complex expression which can be easily decomposed into real and imaginary part. From Equations (8b,c) we got, for the real part,

$$-2x_c\alpha + \frac{ky_q}{\zeta_a^{(q)}} \Rightarrow y_q = 2x_c \frac{\alpha}{k} \zeta_a^{(q)} \tag{12}$$

For the, imaginary part, we got

$$x_c(-2\beta + k\zeta_b^{(q)}) + k\zeta_c^{(q)}x_q \Rightarrow x_q = -x_c \frac{(-2\beta + k\zeta_b^{(q)})}{k\zeta_c^{(q)}} \tag{13}$$

The form of coefficients $\zeta_a^{(q)}, \zeta_b^{(q)}, \zeta_c^{(q)}$ depends on the value of q .

$$\zeta_a^{(q)} = z_1z_2z_3 \dots z_q\gamma_2 \dots \gamma_q \tag{14a}$$

$$\zeta_b^{(1)} = 0, \text{ otherwise } \zeta_b^{(q)} = \frac{1}{z_1^2\gamma_2} + \frac{1}{z_1^2z_2^2\gamma_2^2\gamma_3} + \dots + \frac{1}{z_1^2 \dots z_{q-1}^2\gamma_2^2 \dots \gamma_{q-1}^2\gamma_q} \tag{14b}$$

$$\zeta_c^{(q)} = \frac{1}{z_1 \dots z_q\gamma_2 \dots \gamma_q} \tag{14c}$$

For example for $q = 4$ we get

$$\zeta_a^{(4)} = z_1z_2z_3z_4\gamma_2\gamma_3\gamma_4 \tag{15a}$$

$$\zeta_b^{(4)} = \frac{1}{z_1^2\gamma_2} + \frac{1}{z_1^2z_2^2\gamma_2^2\gamma_3} + \frac{1}{z_1^2z_2^2z_3^2\gamma_2^2\gamma_3\gamma_4} \tag{15b}$$

$$\zeta_c^{(4)} = \frac{1}{z_1z_2z_3z_4\gamma_2\gamma_3\gamma_4} \tag{15c}$$

Formulas in Equations (12) and (13) show that y-coordinate is a member of imaginary part and x-coordinate is a member of real part of the $B_x + iB_y$ expression. This leads us to simple formulas for

vortex point trajectory. The vortex point (zero amplitude point) is at the place where both imaginary and real part are equal to zero [1–3].

$$-2x_c\alpha + \frac{ky_q}{\xi_a^{(q)}} = 0 \Rightarrow y_q = 2x_c \frac{\alpha}{k} \xi_a^{(q)} \tag{16a}$$

$$x_c (-2\beta + k\xi_b^{(q)}) + k\xi_c^{(q)}x_q = 0 \Rightarrow x_q = -x_c \frac{(-2\beta + k\xi_b^{(q)})}{k\xi_c^{(q)}} \tag{16b}$$

From the above formula we may conclude that the vortex trajectory as a function of x_c , for the given z is a straight line. We may also find a plane where the vortex trajectory is perpendicular to the SPP shift. Using Equation (16b) the condition is

$$x_q = 0 \Rightarrow -2\beta + k\xi_b^{(q)} = 0 \tag{17}$$

In the paper [52] we have formulated the hypothesis that the higher order vortices ($m > 1$) do not split even when $x_c \neq 0$. The higher order vortices are classified as structurally unstable [62], i.e., they are supposed to split into single order vortices even under small phase or amplitude perturbation [63–65]. Nevertheless, the formulas in Equation (11) proof the stability hypothesis in an explicit form. The factors in front of the Kummer confluent hypergeometric function are just a vortex term.

$$\left(\frac{B_x^{(q)}}{2\sqrt{-A^{(q)}}} + i \frac{B_y^{(q)}}{2\sqrt{-A^{(q)}}} \right)^m \tag{18}$$

The place where the real and imaginary part of $B_x^{(q)} + iB_y^{(q)}$ is zero indicates the position of the vortex point of the m -th order. Since the whole term is at power m , the m -order vortex does not split for any x_c . The result is very interesting, which is illustrated in Figure 4.

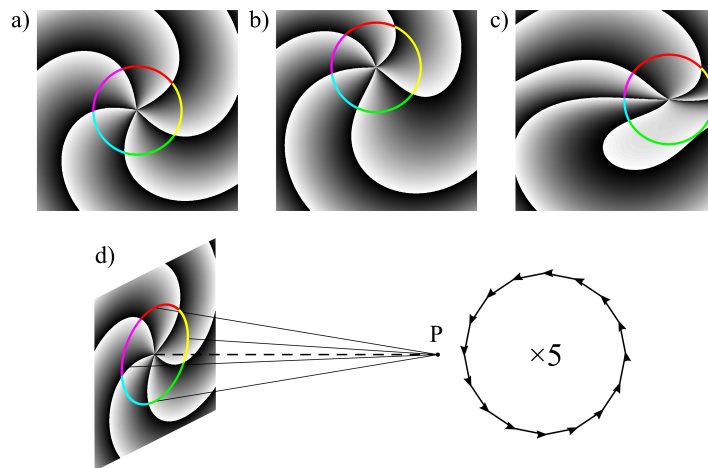


Figure 4. (a) The phase distribution of the optical vortex beam ($m = 5$) for $x_c = 0$ as seen just behind the SPP. Part (d) shows the sum of phasors calculated at point P (at image plane) on the optical axis, while going along the colored circle. Due to symmetry and 2π phase change along the green part of the circle the phasors (from the green part) form a full circle at sum up to zero. Going along the parts marked with different colors will produce five such circles of phasors, at the same place, which again sum to zero; (b) when $x_c \neq 0$, the symmetry breaks. In a typical case each part of the circle noted by different color will form zero at different point at the image plane, splitting the m -th order vortex into a set of single vortices. However, our case is untypical and the higher order vortex does not split; (c) when performing more complex operation as described below, we will produce even less symmetrical phase distribution, but the higher order vortex is still stable.

The situation would not be strange if the higher order optical vortex were stable for a given non-zero value x_c . However, changing the x_c continuously breaks the circular symmetry of the phase distribution at the SPP plane with no harm for the higher order OV stability. We could also start our analysis at the sample plane, where both phase and amplitude distribution symmetry are broken (Figure 5). Nevertheless, the propagation of this input beam through any number of lenses will not split the higher order vortices. In paper [55] similar results were obtained for a simpler system, i.e., Gaussian beam illuminating the off-axis SPP.

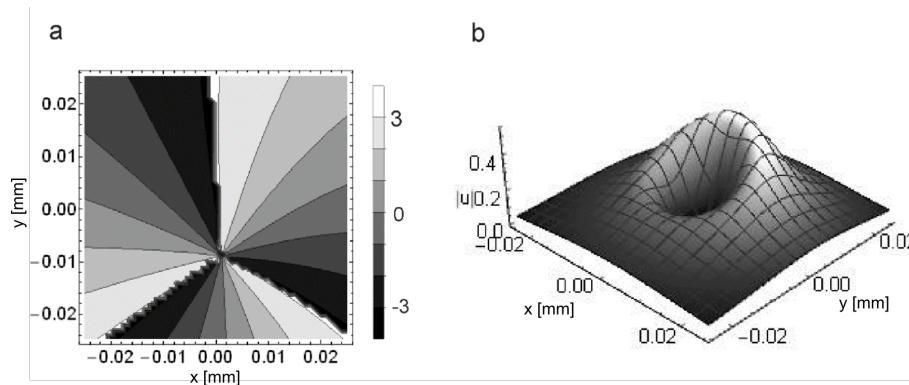


Figure 5. The vortex beam of $m = 3$ focused by the lens $f_1 = 15$ mm (according to Figure 2a); (a) phase and (b) amplitude distribution, calculated at $z = 14.88$ mm. Both distributions are evidently asymmetrical ($x_c = 0.15$ mm). Nevertheless, they do not split while propagating through the rest of the OVSM system.

We can go even further. Adding the term inside the bracket in Equation (18) and multiplying B_x or B_y coefficients by any number, but in such a way that the coefficients by $x_{(q)}$ remain real (or become imaginary) and coefficient by $y_{(q)}$ remains imaginary (or becomes real) may change the position of the vortex point and its phase distribution (Figure 5c) but still the higher order vortices will be stable while propagating through our system. However, changing other parameters, like, for example, binomial factor by coefficients B in Equation (5) splits the higher order vortices immediately (Figure 6).

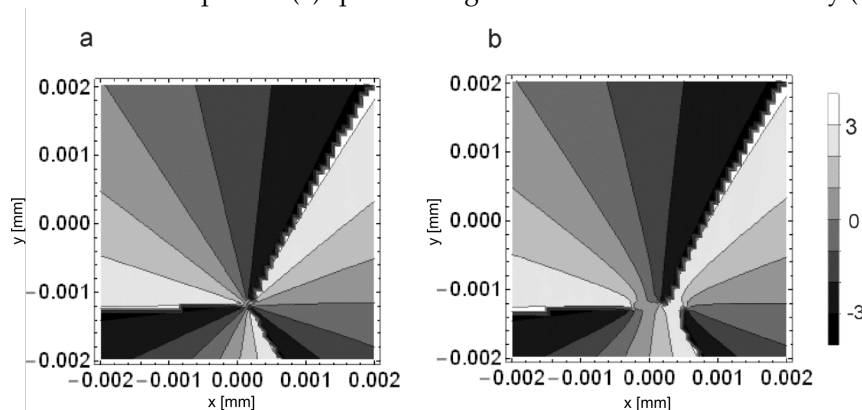


Figure 6. The phase image of focused vortex beam (parameters as in Figure 2b), $m = 3$; (a) calculated from Kappa function with $n = 21$. The higher order vortex is still there; (b) calculated from Kappa function with $n = 21$, but the number 0.05 was added to binomial factor in the second sum for $n = 1$. The vortex was split into three single vortices.

To summarize this part: We have shown that the higher order vortices when propagating through the set of classical lenses described in paraxial approximation will not split regardless of asymmetry introduced by the off axis position of the SPP. Moreover, we may perform some more symmetry breaking operation (as shown in Figure 4c) in Equation (8c,d), provided that the coefficients by x remain real (or imaginary) and by y imaginary (or real). So, the conclusion is that the very basic optical

system does not split the higher order vortices even if the input phase and amplitude distribution is highly non-symmetrical. In many cases, such an unusual stability results from deeper physical rules. There is a question if this is also a case here. So far we have no answer to this question. What we can learn now is that classical optical system is somewhat special, at least when being described in paraxial approximation and illuminated by Gaussian beam with the vortex beam introduced by SPP. In the next section the special role of the coefficient A will be studied.

3. Coefficient A

In our further discussion we will refer to two specific examples of the OVSM models. One with the separated SPP plate and focusing lens (Figure 2a) and the second one with SPP plate and focusing lens working as single thin element (Figure 2b).

The coefficient $A^{(q)}$ has relatively simple form. It depends neither on the x and y coordinates nor on SPP shift x_c . However, it plays a crucial role in vortex beam phase evolution. Unfortunately it cannot be totally taken outside the first sum in Kappa function. On the contrary, in Equation (4) it can be entirely assimilated inside the first sum, but in the present form some mathematical aspects can be noticed in a more clear way.

The first important point is that the coefficient A is responsible for breaking the Kappa function convergence. In the OVSM this happens when the SPP is separated from the focusing lens, and coefficient A has a singular point (Figure 7a,b). At first we will analyze the system with two blocks, the SPP and the focusing lens (sample plane is an observation plane in this case), so we need the second order coefficient $A^{(2)}$. The coefficient $A^{(q)}$ contributes to the Kappa function as $1/A^{(q)}$, so the term in front of the first sum takes form (for $q = 2$).

$$\frac{1}{A^{(2)}} = \left(\alpha + i\beta - \frac{ik}{2z_1^2\gamma_2} \right)^{-1} \quad (19)$$

There exists a range of such positive z_2 for which the conditions in Equation (9) fail. In particular there is a z_2 value that the γ_2 equals zero and the whole term in Equation (19) becomes zero. Thus, the whole Kappa function is equal to zero, which shows that it does not reflect the true behavior of the focused vortex beam. Moreover, the Kappa function encounters a π -jump in this point. This z_2 value can be computed from the formula

$$z_2 = \frac{z_1 f_2}{f_2 - z_1} \quad (20)$$

Figure 7a,b illustrates the problem. As we can see for the $z_2 = 15.58$ mm (calculated from Equation (20)) the $1/A^{(2)}$ term equals zero.

When the SPP and focusing lens are joined, we only need a coefficient $A^{(1)}$ which has a simple form, free of our problem (at least for the OVSM optical system). This is illustrated in Figure 7c,d. The higher order terms $A^{(q)}$ ($q > 2$) behave in a similar way. When the SPP and focusing lens work as a single element, they meet the conditions in Equation (9), for a reasonable OVSM configuration. When $q > 2$ the set of conditions in Equation (9) is more complicated. The detailed study of this problem would explode the volume of this paper, so we will not follow this path. Importantly, when the SPP and focusing lens work separately, the condition in Equation (9) fails for any $q > 1$ in case of reasonable OVSM configurations. From a practical point of view, it is enough to check if the $A^{(q)}$ factor behaves like in Figure 7c,d, which is the case in the system shown in Figure 2b. It is worth noticing here that when using the ISM, all $z_{(q)}$ parameters are fixed, so the test for conditions in Equation (9) is not difficult. When we move any element of our system along the optical axis the conditions in Equation (9) have to be checked for the whole range of $z_{(q)}$ coordinates.

For the reason explained above we cannot use our formulas to the system shown in Figure 2a. Instead, we have to limit our study to the system shown in Figure 2b, when both SPP and focusing

lens work together. Certainly for the forbidden area the numerical modeling of our optical system is still possible and effective.

We can also find $A^{(q)}$ coefficient inside the first sum in Kappa function. Now, we multiply this term by $1/A$, located in front of the first sum, so we have

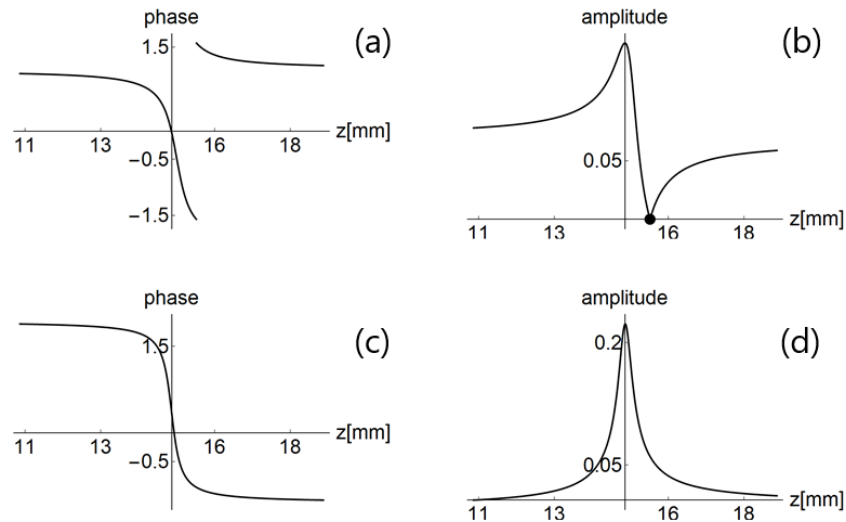


Figure 7. The phase (a) and amplitude (b) distribution of the $1/A^{(2)}$ in case of system with the separated SPP and focusing lens as a function of focusing lens position in respect to the sample plane. In (c,d) the phase and amplitude distribution of the $1/A^{(1)}$ term is shown in case of SPP and focusing lens working as a single element (with no separation).

$$\frac{1}{\left((-A^{(q)})^{\frac{3}{2}}\right)^{2n+1}}; \text{for } q \text{ odd} \tag{21a}$$

$$\frac{1}{\left((-A^{(q)})^{\frac{3}{2}}\right)^{2n+2}}; \text{for } q \text{ even} \tag{21b}$$

The first term (for $n = 0$) has the largest influence on the phase and amplitude of the Kappa function. The next terms rapidly drop in their values. The plot in Figure 8 is done for $q = 4$, but it represents the typical curve for expressions in Equation (21a,b) for any q , provided that we avoid the forbidden area defined by conditions (9). As we can see the part for $n = 0$ strongly dominates over the part for $n = 1$. The next terms (for $n = 2, 3, \dots$) are invisible in the figure scale. This domination is particularly strong at the beam center, when $x_{(q)}$ and $y_{(q)}$ coordinates are small (Figure 3). When the $x_{(q)}$ and $y_{(q)}$ become larger, the coefficient grows rapidly with increasing n and things become more complicated.

Figure 7c suggests that the $A^{(q)}$ coefficient may play a primary role in phase evolution after the SPP, i.e., when changing the position of any element behind the SPP or SPP and focusing lens themselves. This is illustrated in Figure 9a. If $A^{(1)} = 1$ and $x_c = 0$, there is no phase rotation when changing the position of the focusing lens along the z -axis. We can conclude that in the OVSM system the coefficient $A^{(q)}$ plays, in some respect, the similar role as the Gouy phase in the Gaussian beam. When the $x_c \neq 0$ things become more complicated. The off-axis position of the SPP plate introduces a phase value dependence on x_c being inside the coefficient B_x (Figure 9b).

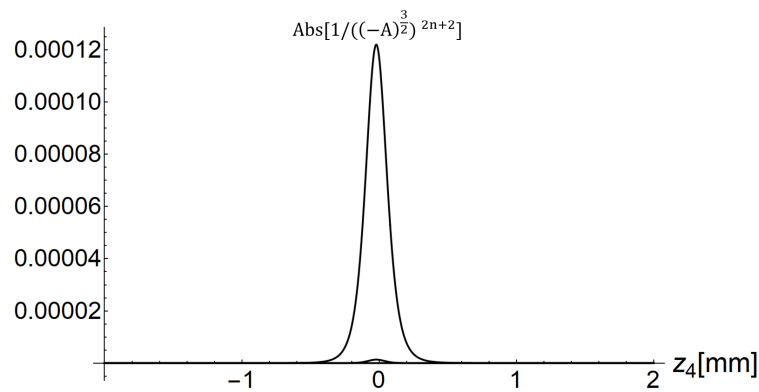


Figure 8. The absolute value of the Equation (21b) containing $A^{(4)}$ coefficient for two values of $n = 0$ and $n = 1$, in case of even topological charge. For growing n the absolute value drops rapidly. So for $n = 1$ the maximum value is 1.2×10^{-4} and the plot is hardly visible in this figure. As a result, the $n = 0$ coefficient play a major role in the Kappa function. For $n = 2$ the maximum value is 1.3×10^{-6} . For any next n the maximum value decreases by two orders.

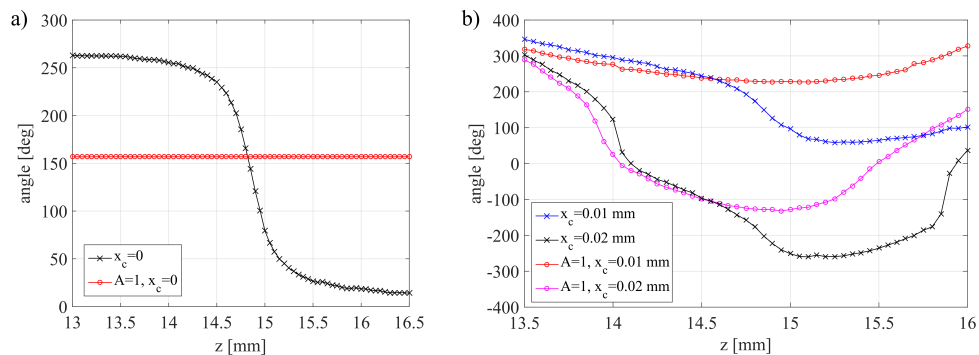


Figure 9. (a) The phase rotation in case of $A^{(1)}$ in full form and when $A^{(1)} = 1$, but for $x_c = 0$; (b) The same, but $x_c \neq 0$.

The other coefficients (but B_x, B_y) play minor role. The coefficient B_x and B_y are responsible for the vortex trajectory evolution as a function of SPP shift x_c . This dependence is linear, but as has been already shown, the direction of vortex trajectory becomes perpendicular to SPP trajectory when the condition in Equation (17) holds. In the previous papers [52,53] this fact was proved for the small x_c . Having the formulas in Equation (11) we can conclude that they hold for any x_c . In paper [59] precise experiments were reported which confirm the theoretical results.

The coefficient Ξ_q collects all constant factors. It must be observed when we analyze the rotation of the beam phase while moving the first block in the optical system along the z -axis. When the first element moves away or toward the laser source, the phase of the incident Gaussian beam changes. This incident phase is a part of coefficient Ξ_q .

The coefficient $C^{(q)}$ multiplies the first sum in function Kappa. Due to the $(x_q^2 + y_q^2)$ factor, the C coefficient is responsible for the equiphase lines curvature (Figure 10). When $C^{(q)} = 1$ the equiphase lines are straight (for $x_c = 0$). Since the $C^{(q)}$ coefficient contributes to the Kappa function as $\exp(x_c^2 \alpha + i\Lambda)$, where Λ is an imaginary part of the C coefficient, and typically $\alpha \ll \Lambda$ its contribution to the amplitude is small, especially for small x_c .

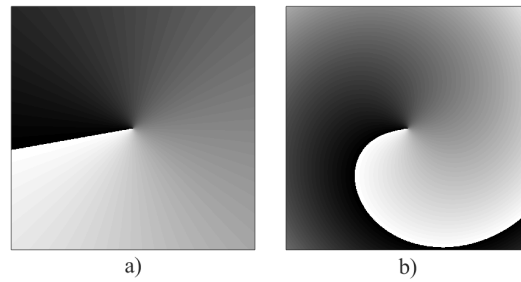


Figure 10. The exemplary phase distribution of the vortex beam in case of (a) $C^{(q)} = 1$ and (b) full $C^{(q)}$ coefficient.

4. The Ice-Skater Effect

To see the effectiveness of our formulas we study the correlation between the focused beam radius and vortex trajectory rotation (see the inset in Figure 1). The hypothesis was that the vortex trajectory behaves like a rigid body. Consequently we assumed that in the closed system of a focused vortex beam the angular momentum L is conserved, thus $L = I\omega = const$. Regardless of the assumed model (point mass, flat disk, cylinder, etc.), the moment of inertia I is always proportional to the squared distance r from the rotation axis, i.e., $I \approx r^2$. Therefore, the rotational speed ω of the vortex trajectory shall satisfy $\omega \approx 1/r^2$. In our case, ω is the first derivative of the trajectory inclination angle with respect to z ($\omega = d\theta/dz$) and r is the radius of the vortex bright ring, i.e., the distance between points of zero and maximal intensity (e.g., $r = 2.1$ mm for the vortex analyzed in Figure 3). Both the radius of the converging vortex beam and the rotational speed of the trajectory depend on the axial distance z . Obviously, as z approaches the focal point, the vortex radius decreases whereas the rotations speed up. As the beam focusses, the radius reaches its minimum and the speed is maximal. This is a direct analogy to the ice skater pulling their arms in for a faster spin. Such a rigid body mechanics approach to the vortex beam has been already studied by Bekshaev et al. [11], for free propagating Gaussian beam with optical vortex. The authors concluded that it is related to the Gouy phase dynamics. We have stated that the coefficient A plays the role of the Gouy phase in our case. Indeed, from Equations (12) and (13) we may calculate the angle of the trajectory inclination as

$$\tan(\phi_{(q)}) = \frac{y_{(q)}}{x_{(q)}} = -2 \frac{\alpha}{(-2\beta + k\tilde{z}_b^{(q)})} \tag{22}$$

For $q = 1$ we get

$$\tan(\phi_{(q)}) = \frac{\alpha}{\beta} \tag{23}$$

Calculating the angle of the equiphase line for the A coefficient we get exactly the same formula.

Here we present the results calculated at the exit of the setup (camera plane) shown in Figure 2b. The default z -position is where the the focal point of the beam lies very close to the critical plane (plane where the trajectory is perpendicular to the SPP shift x_c). Defocusing is performed by moving the focusing objective along the optical axis without changing the position of other elements. Thus, the plane at which the vortex beam is imaged is at different distances from the focus resulting in different vortex radii, as shown in Figure 11a. These calculations require running the Kappa function once for each point on the graph. On the other hand, computing the vortex trajectory rotation speed ω is much easier. In paper [39] the formula for ω was given as:

$$\omega = \frac{2kw^2(z)}{4z_0^2 + k^2w^4(z) \left(1 - z_0 \left(\frac{1}{R(z)} + \frac{1}{f}\right)\right)^2} \tag{24}$$

In fact the formula in Equation (24) was derived for the vortex trajectory rotation at the sample plane for the approximated linear case ($n = 0$). However, the new formulas in Equation (11) allow to extent their applicability for general case. The classical imaging preserves the vortex trajectory orientation as was shown experimentally in [53,58]. So we expect that the angle rotation at the image plane is the same as in the sample plane.

The obtained relation between the rotational speed and the defocusing is presented in Figure 11b, red. Applying the above rigid-body reasoning, ω was compared with the inverse square of the vortex radius (Figure 11b, black). There is a clear agreement between the two curves supporting the hypothesis of rigid-like behavior of vortex trajectory.

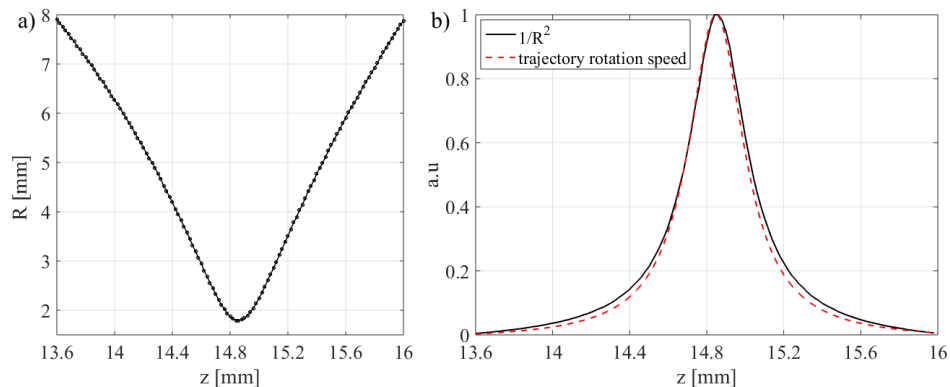


Figure 11. (a) The radius R of the focused optical vortex ($m = 1$) calculated using Kappa function for the setup in Figure 2b. The radius is minimal at the focal point ($z = 14.86$ mm); (b) The rotational speed of the vortex trajectory (red) calculated using Equation (24) compared with the inverse square of R (black). The height of the curves was normalized to 1. Parameters used in both calculations: $w_0 = 0.4$ mm, $z_G = 600$ mm, $\lambda = 630$ nm.

5. Discussion

There is a growing interest in the exact theory describing the propagation of the optical vortex beams in the optical system, in particular in a system with broken symmetry. The reasons are both understanding the physics of electromagnetic waves (also in quantum picture) and practical applications. Some examples concerning both science or applications can be found in [11,14,24,33,34,55,57,59,63,65–67], but the list of papers is much longer. In this paper we have enhanced the results presented in our former works [52,53]. The Kappa function describing our system can be applied for any numbers of lenses. We have derived the coefficient for Kappa function for any numbers of elements. We have also enhanced the formulas for the vortex trajectory. Moreover, we have found a closed form of our solution in Equation (11) using the special function. This new form proved that in classical optical system the higher order vortices do not split even if the circular symmetry is broken. This is true under the conditions of paraxial approximation. This result is surprising and it is hard to check it experimentally. We cannot use an optical system in paraxial approximation. Moreover, any real system introduces errors which break the beam symmetry in a way different than allowed by our theory. This immediately splits the higher order vortices forming a constellation of the first order ones. Nevertheless, the experiment reported in [52] suggested the mass center of such a constellation moves as ideal higher order vortex. There is also an open question: what is the reason for such a special behavior?

The study on $A^{(q)}$ coefficient have shown that it is responsible for breaking the conditions in Equation (9). As a result, we cannot analyze the OVSM system with separated SPP plate and focusing lens. The $A^{(q)}$ coefficient has an important role in the rotation of vortex beam phase, which is similar to the role of the Gouy phase in Gaussian beam. The second important factor is the SPP shift x_c . When we are close to vortex core we can limit the sum range (in Kappa function) to $n = 0$, which is also the result of the $A^{(q)}$ coefficient specific behavior (Figure 8).

We have shown that the vortex trajectory behaves like a rigid body. The range of the trajectory shrinks when the beam converge, so its rotation speed increases according to the rules describing the rigid body behavior. The vortex trajectory rotation is strictly related to the phase rotation of the $A^{(q)}$ coefficient. In [11] the same relation was shown for free propagation of axial Gaussian vortex beam and the Gouy phase. It is worth noticing here that our theoretical results concerning the vortex trajectory dynamics as well as the shape of the beam at the observation plane were in agreement with numerical simulations performed with the software dedicated for solving diffraction problems.

The question is if we can enhance our results for more general optical systems like, for example, the system generating Laguerre–Gaussian beam with the SPP of the special profile [28]. There are various types of vortex beams which are studied for their practical potential in optical metrology, manipulation and telecommunication. Unfortunately, we have not found any general way for transforming our results to a wider class of possible vortex beams. So far any system variation generates difficult diffraction problems which must be solved separately.

6. Conclusions

In this work the problem of the optical vortex beam propagation through the system of lenses was solved analytically and core derivations were presented. The solution can be expressed either as a series or in a closed form using Kummer confluent hypergeometric function. The formulas are applicable to any integer vortex charge and any number of lenses in the optical setup. Here, the setup of interest was the optical vortex scanning microscope. Moreover, the expressions hold for the off-axis spiral phase plate (used for vortex generation) which results in broken circular symmetry of the intensity and phase distribution. Analytical results supported by numerical calculations led to three key findings. First, in paraxial approximation in both symmetric and asymmetric case the higher order vortices do not split as they immediately do in real (non-ideal) systems. Second, one of the four main coefficients in the derived solution determines the phase rotations of the vortex beam and thus acts analogously to the Gouy phase in the standard Gaussian beam. Lastly, the rotational speed of vortex trajectory is inversely proportional to the vortex radius and was thus proved to behave like a rigid body. The bottom line is that the obtained analytical formulas are a ready-made tool for extensive research in vortex beam propagation dynamics.

Appendix A

In this section we will prove a recursive formulas in Equation (8) by mathematical induction. The first step is verification for $q = 2$, which has been already done in the previous paper [58].

$$u_2(x_2, y_2) = \Xi_2 \frac{2i\pi}{k\gamma_2} K(A^{(2)}, B_x^{(2)}, B_y^{(2)}, C^{(2)}) \tag{A1}$$

Next we assume that the formula is correct

$$u_j(x_j, y_j) = \Xi_j \left(\frac{2i\pi}{k} \right)^{j-1} \prod_{s=1}^j \frac{1}{\gamma_s} K(A^{(j)}, B_x^{(j)}, B_y^{(j)}, C^{(j)}) \tag{A2}$$

Finally, we have to prove the implication

$$u_j(x_j, y_j) \Rightarrow u_{j+1}(x_{j+1}, y_{j+1}) \tag{A3}$$

We can write a right side of the implication as

$$u_{j+1}(x_{j+1}, y_{j+1}) = \zeta_{j+1} \iint_{\mathbb{R}^2} u_j(x_j, y_j) e^{\frac{ik}{2z_{j+1}}(x_{j+1}^2 + y_{j+1}^2)} e^{\frac{ik}{2z_{j+1}}(x_j^2 + y_j^2)} e^{-\frac{ik}{2f_{j+1}}(x_j^2 + y_j^2)} \times e^{-\frac{ik}{z_{j+1}}(x_{j+1}x_j + y_{j+1}y_j)} dx_j dy_j \tag{A4}$$

After plugging the definition of u_j into the integral to obtain

$$\begin{aligned}
 u_{j+1}(x_{j+1}, y_{j+1}) = & \zeta_{j+1} \iint_{\mathbb{R}^2} \Xi_j \left(\frac{2i\pi}{k} \right)^{j+1} \prod_{s=1}^j \frac{1}{\gamma_s} \left[\iint_{\mathbb{R}^2} e^{im\text{Arg}(x_0+iy_0)} \right. \\
 & \times e^{-\left(\frac{1}{w^2(z)} + \frac{ik}{2R(z)}\right) [(x_0-x_c)^2+y_0^2]} e^{-\frac{ik}{2f_1} [(x_0-x_c)^2+y_0^2]} e^{\frac{ik}{2z_1} [(x_0-x_c)^2+y_0^2]} \\
 & \times e^{-\frac{ik}{2\gamma_2} \left[\left(\frac{x_0-x_c}{z_1}\right)^2 + \left(\frac{y_0}{z_1}\right)^2 \right]} e^{-\frac{ik}{2\gamma_3} \left[\left(\frac{x_0-x_c}{z_1 z_2 \gamma_2}\right)^2 + \left(\frac{y_0}{z_1 z_2 \gamma_2}\right)^2 \right]} e^{-\frac{ik}{2\gamma_4} \left[\left(\frac{x_0-x_c}{z_1 z_2 z_3 \gamma_2 \gamma_3} + \frac{x_4}{z_4}\right)^2 + \left(\frac{y_0}{z_1 z_2 z_3 \gamma_2 \gamma_3} + \frac{y_4}{z_4}\right)^2 \right]} \\
 & \times \dots e^{-\frac{ik}{2\gamma_{j-1}} \left[\left(\frac{x_0-x_c}{\prod_{s=1}^{j-2} z_s \gamma_s}\right)^2 + \left(\frac{y_0}{\prod_{s=1}^{j-2} z_s \gamma_s}\right)^2 \right]} e^{-\frac{ik}{2\gamma_j} \left[\left(\frac{x_0-x_c}{\prod_{s=1}^{j-1} z_s \gamma_s} + \frac{x_j}{z_j}\right)^2 + \left(\frac{y_0}{\prod_{s=1}^{j-1} z_s \gamma_s} + \frac{y_j}{z_j}\right)^2 \right]} \left. dx_0 dy_0 \right] \\
 & \times e^{\frac{ik}{2z_{j+1}} (x_{j+1}^2+y_{j+1}^2)} e^{\frac{ik}{2z_{j+1}} (x_j^2+y_j^2)} e^{-\frac{ik}{2f_{j+1}} (x_j^2+y_j^2)} e^{-\frac{ik}{z_{j+1}} (x_{j+1}x_j+y_{j+1}y_j)} dx_j dy_j
 \end{aligned} \tag{A5}$$

By interchanging the order of integration we can write

$$\begin{aligned}
 u_{j+1}(x_{j+1}, y_{j+1}) = & \Xi_{j+1} \left(\frac{2i\pi}{k} \right)^{j+1} \prod_{s=1}^j \frac{1}{\gamma_s} \iint_{\mathbb{R}^2} e^{im\text{Arg}(x_0+iy_0)} \\
 & \times e^{-\left(\frac{1}{w^2(z)} + \frac{ik}{2R(z)}\right) [(x_0-x_c)^2+y_0^2]} e^{-\frac{ik}{2f_1} [(x_0-x_c)^2+y_0^2]} e^{\frac{ik}{2z_1} [(x_0-x_c)^2+y_0^2]} e^{\frac{ik}{2z_{j+1}} (x_{j+1}^2+y_{j+1}^2)} \\
 & \times e^{-\frac{ik}{2\gamma_2} \left[\left(\frac{x_0-x_c}{z_1}\right)^2 + \left(\frac{y_0}{z_1}\right)^2 \right]} e^{-\frac{ik}{2\gamma_3} \left[\left(\frac{x_0-x_c}{z_1 z_2 \gamma_2}\right)^2 + \left(\frac{y_0}{z_1 z_2 \gamma_2}\right)^2 \right]} e^{-\frac{ik}{2\gamma_4} \left[\left(\frac{x_0-x_c}{z_1 z_2 z_3 \gamma_2 \gamma_3} + \frac{x_4}{z_4}\right)^2 + \left(\frac{y_0}{z_1 z_2 z_3 \gamma_2 \gamma_3} + \frac{y_4}{z_4}\right)^2 \right]} \\
 & \times \dots e^{-\frac{ik}{2\gamma_{j-1}} \left[\left(\frac{x_0-x_c}{\prod_{s=1}^{j-2} z_s \gamma_s}\right)^2 + \left(\frac{y_0}{\prod_{s=1}^{j-2} z_s \gamma_s}\right)^2 \right]} e^{-\frac{ik}{2\gamma_j} \left[\left(\frac{x_0-x_c}{\prod_{s=1}^{j-1} z_s \gamma_s}\right)^2 + \left(\frac{y_0}{\prod_{s=1}^{j-1} z_s \gamma_s}\right)^2 \right]} \\
 & \times \left[\iint_{\mathbb{R}^2} e^{-\frac{ik}{2\gamma_j z_j} \left(\frac{2(x_0-x_c)x_j}{\prod_{s=1}^{j-1} z_s \gamma_s} + \frac{2y_0 y_j}{\prod_{s=1}^{j-1} z_s \gamma_s} \right)} e^{-\frac{ik}{2z_j^2 \gamma_j} (x_j^2+y_j^2)} \right. \\
 & \left. \times e^{\frac{ik}{2z_{j+1}} (x_{j+1}^2+y_{j+1}^2)} e^{-\frac{ik}{2f_{j+1}} (x_{j+1}^2+y_{j+1}^2)} e^{-\frac{ik}{z_{j+1}} (x_{j+1}x_j+y_{j+1}y_j)} dx_j dy_j \right] dx_0 dy_0
 \end{aligned} \tag{A6}$$

The integral in the parentheses is Gaussian and thus can be computed explicitly using the formula

$$\int_{-\infty}^{\infty} e^{i\sigma x^2 - i\mu x} dx = \sqrt{\frac{\pi}{-i\sigma}} e^{-\frac{i\mu^2}{4\sigma}} \tag{A7}$$

Eventually, we can write

$$u_{j+1}(x_{j+1}, y_{j+1}) = \Xi_{j+1} \left(\frac{2i\pi}{k} \right)^{j+1} \prod_{s=1}^j \frac{1}{\gamma_s} K(A^{(j+1)}, B_x^{(j+1)}, B_y^{(j+1)}, C^{(j+1)}) \tag{A8}$$

Appendix B

In this section we will prove the formula in Equation (10).

In the first step the formula for positive vortex charge can be written as

$$u_{j+}(x_j, y_j) = \Xi_j K(A^{(j)}, B_x^{(j)}, B_y^{(j)}, C^{(j)}) \tag{A9}$$

Similarly, the formula for negative vortex charge is

$$u_{j-}(x_j, y_j) = \Xi_j \iint_{R^2} e^{im\phi} e^{A^{(j)}\rho^2 + B_x^{(j)}\rho \cos \phi + B_y^{(j)}\rho \sin \phi + C^{(j)}} \rho d\rho d\phi \tag{A10}$$

Then, we substitute $\theta = 2\pi - \phi$ for integration over θ , we have

$$\Xi_j e^{im2\pi} \iint_{R^2} e^{-im\theta} e^{A^{(j)}\rho^2 + B_x^{(j)}\rho \cos \theta - B_y^{(j)}\rho \sin \theta + C^{(j)}} \rho d\rho d\theta \tag{A11}$$

Finally, we can write

$$u_{j-}(x_j, y_j) = -e^{-im2\pi} \Xi_j K(A^{(j)}, B_x^{(j)}, -B_y^{(j)}, C^{(j)}) \tag{A12}$$

Appendix C

In this section we will prove the formula in Equation (11).

Using polar coordinates in formula Equation (1) we have

$$u(x_1, y_1) = \int_0^{2\pi} e^{im\phi} d\phi \int_0^\infty e^{A\rho^2 + B_x\rho \cos \phi + B_y\rho \sin \phi + C} \rho d\rho \tag{A13}$$

Integrating over the radius we have

$$\int_0^\infty e^{-\gamma\rho^2 - \sigma\rho} \rho d\rho = \frac{1}{2\gamma} \left[1 - \sqrt{\pi} \frac{\sigma}{2\sqrt{\gamma}} e^{\frac{\sigma^2}{4\gamma}} \left(1 - \operatorname{erf} \left(\frac{\sigma}{2\sqrt{\gamma}} \right) \right) \right] \tag{A14}$$

After integration we get

$$u(x_1, y_1) = -\frac{e^C}{2A} \int_0^{2\pi} \left[1 - \sqrt{\pi} \frac{-(B_x \cos \phi + B_y \sin \phi)}{2\sqrt{-A}} e^{-\frac{(B_x \cos \phi + B_y \sin \phi)^2}{4A}} \right. \\ \left. \times \left(1 - \operatorname{erf} \left(\frac{-(B_x \cos \phi + B_y \sin \phi)}{2\sqrt{-A}} \right) \right) \right] e^{im\phi} d\phi \tag{A15}$$

After calculating the sum we have

$$u(x_1, y_1) = -\frac{\sqrt{\pi}e^C}{2\sqrt{-A}} \sum_{n=\frac{m-1}{2}}^\infty \frac{1}{n!} \frac{\pi}{2^{2n}} \binom{2n+1}{n+\frac{m+1}{2}} \\ \times \left(\frac{B_x}{2\sqrt{-A}} + i\frac{B_y}{2\sqrt{-A}} \right)^{n+\frac{m+1}{2}} \left(\frac{B_x}{2\sqrt{-A}} - i\frac{B_y}{2\sqrt{-A}} \right)^{n-\frac{m-1}{2}}; \text{ for } m \text{ odd} \tag{A16}$$

$$u(x_1, y_1) = \frac{e^C}{2\sqrt{-A}} \sum_{n=\frac{m}{2}-1}^\infty \frac{2^{n+1}}{(2n+1)!!} \binom{2n+2}{n+1+\frac{m}{2}} \\ \times \left(\frac{B_x}{2\sqrt{-A}} + i\frac{B_y}{2\sqrt{-A}} \right)^{n+1+\frac{m}{2}} \left(\frac{B_x}{2\sqrt{-A}} - i\frac{B_y}{2\sqrt{-A}} \right)^{n+1-\frac{m}{2}}; \text{ for } m \text{ even} \tag{A17}$$

Finally, we can write

$$u(x_1, y_1) = -\frac{\pi\sqrt{\pi}e^C}{2^m\sqrt{-A}} \frac{1}{\left(\frac{m-1}{2}\right)!} \left(\frac{B_x}{2\sqrt{-A}} + i\frac{B_y}{2\sqrt{-A}} \right)^m \\ \times {}_1F_1 \left(1 + \frac{m}{2}, 1 + m, \left(\frac{B_x}{2\sqrt{-A}} \right)^2 + \left(\frac{B_y}{2\sqrt{-A}} \right)^2 \right); \text{ for } m \text{ odd} \tag{A18}$$

$$u(x_1, y_1) = \frac{\pi e^C}{2^{\frac{m}{2}} \sqrt{-A}} \frac{1}{(m-1)!!} \left(\frac{B_x}{2\sqrt{-A}} + i \frac{B_y}{2\sqrt{-A}} \right)^m \quad (\text{A19})$$

$$\times {}_1F_1 \left(1 + \frac{m}{2}, 1 + m, \left(\frac{B_x}{2\sqrt{-A}} \right)^2 + \left(\frac{B_y}{2\sqrt{-A}} \right)^2 \right); \text{ for } m \text{ even}$$

Author Contributions: Conceptualization, J.M.; methodology, I.A. and Ł.P.; formal analysis, J.M., I.A. and W.L.; investigation, W.L., I.A. and A.P.-M.; writing—original draft preparation, J.M., I.A. and W.L.; writing—review and editing, I.A., J.M., W.L., Ł.P. and A.P.-M.; visualization, W.L. and J.M. All authors have read and agreed to the published version of the manuscript.

Funding: This research received no external funding.

Conflicts of Interest: The authors declare no conflict of interest.

References

1. Vasnetsov, M.; Staliunas, K. *Optical Vortices*; Nova Science: Hauppauge, NY, USA, 1999.
2. Soskin, M.; Vasnetsov, M. Singular optics. *Prog. Opt.* **2001**, *42*, 219–276.
3. Dennis, M.R.; O’Holleran, K.; Padgett, M.J. Singular optics: Optical vortices and polarization singularities. *Prog. Opt.* **2009**, *53*, 293–363.
4. Kotlyar, V.V.; Kovalev, A.A.; Porfirev, A.P. *Vortex Laser Beams*; CRC Press: Boca Raton, FL, USA, 2018.
5. Arora, R.; Lu, Z. Graphical study of Laguerre-Gaussian beam modes. *IEE Proc.-Microwaves Antennas Propag.* **1994**, *141*, 145–150. [[CrossRef](#)]
6. Masajada, J.; Dubik, B. Optical vortex generation by three plane wave interference. *Opt. Commun.* **2001**, *198*, 21–27. [[CrossRef](#)]
7. Senthilkumaran, P.; Masajada, J.; Sato, S. Interferometry with vortices. *Int. J. Opt.* **2012**, *2012*, 517591. [[CrossRef](#)]
8. Ruben, G.; Paganin, D.M. Phase vortices from a Young’s three-pinhole interferometer. *Phys. Rev. E* **2007**, *75*, 066613. [[CrossRef](#)]
9. Vyas, S.; Senthilkumaran, P. Vortex array generation by interference of spherical waves. *Appl. Opt.* **2007**, *46*, 7862–7867. [[CrossRef](#)]
10. Vasnetsov, M.; Pas’ Ko, V.; Soskin, M. Analysis of orbital angular momentum of a misaligned optical beam. *New J. Phys.* **2005**, *7*, 46. [[CrossRef](#)]
11. Bekshaev, A.Y.; Soskin, M.; Vasnetsov, M. An optical vortex as a rotating body: Mechanical features of a singular light beam. *J. Opt. A: Pure Appl. Opt.* **2004**, *6*, S170. [[CrossRef](#)]
12. Yang, D.; Zhao, J.; Zhao, T.; Kong, L. Generation of rotating intensity blades by superposing optical vortex beams. *Opt. Commun.* **2011**, *284*, 3597–3600. [[CrossRef](#)]
13. Khonina, S.N.; Ustinov, A.V.; Fomchenkov, S.A.; Porfirev, A.P. Formation of hybrid higher-order cylindrical vector beams using binary multi-sector phase plates. *Sci. Rep.* **2018**, *8*, 1–11. [[CrossRef](#)] [[PubMed](#)]
14. Bouchal, P.; Bouchal, Z. Flexible non-diffractive vortex microscope for three-dimensional depth-enhanced super-localization of dielectric, metal and fluorescent nanoparticles. *J. Opt.* **2017**, *19*, 105606. [[CrossRef](#)]
15. Sokolenko, B.; Shostka, N.; Karakchieva, O.; Poletaev, D.; Voytitsky, V.; Halilov, S.; Prisyazhniuk, A.; Ilyasova, A.; Kolosenko, E. Optical vortex phase determination for nanoscale imaging. *J. Physics: Conf. Ser. IOP Publ.* **2018**, *1062*, 012004. [[CrossRef](#)]
16. Szatkowski, M.; Masajada, J.; Augustyniak, I.; Nowacka, K. Generation of composite vortex beams by independent Spatial Light Modulator pixel addressing. *Opt. Commun.* **2020**, *463*, 125341. [[CrossRef](#)]
17. Bazhenov, V.Y.; Soskin, M.; Vasnetsov, M. Screw dislocations in light wavefronts. *J. Mod. Opt.* **1992**, *39*, 985–990. [[CrossRef](#)]
18. Indebetouw, G. Optical vortices and their propagation. *J. Mod. Opt.* **1993**, *40*, 73–87. [[CrossRef](#)]
19. Rozas, D.; Law, C.; Swartzlander, G. Propagation dynamics of optical vortices. *J. Opt. Soc. Am. B* **1997**, *14*, 3054–3065. [[CrossRef](#)]
20. Topuzoski, S.; Janicijevic, L. Diffraction of Laguerre-Gaussian beam by a helical axicon. *Acta Phys. Pol.-Ser. A Gen. Phys.* **2009**, *19*, 557. [[CrossRef](#)]
21. Khonina, S.; Kotlyar, V.; Shinkaryev, M.; Soifer, V.; Uspleniev, G. The phase rotor filter. *J. Mod. Opt.* **1992**, *39*, 1147–1154. [[CrossRef](#)]

22. Beijersbergen, M.; Coerwinkel, R.; Kristensen, M.; Woerdman, J. Helical-wavefront laser beams produced with a spiral phaseplate. *Opt. Commun.* **1994**, *112*, 321–327. [[CrossRef](#)]
23. Allen, L.; Padgett, M.; Babiker, M. The Orbital Angular Momentum of Light. *Prog. Opt.* **1999**, *39*, 291–372.
24. Swartzlander, G.A., Jr. Achromatic optical vortex lens. *Opt. Lett.* **2006**, *31*, 2042–2044. [[CrossRef](#)] [[PubMed](#)]
25. Khoroshun, A.N. Optimal linear phase mask for the singular beam synthesis from a Gaussian beam and the scheme of its experimental realisation. *J. Mod. Opt.* **2010**, *57*, 1542–1549. [[CrossRef](#)]
26. Kotlyar, V.V.; Almazov, A.A.; Khonina, S.N.; Soifer, V.A.; Elfstrom, H.; Turunen, J. Generation of phase singularity through diffracting a plane or Gaussian beam by a spiral phase plate. *J. Opt. Soc. Am. A* **2005**, *22*, 849–861. [[CrossRef](#)]
27. Khonina, S.; Porfirev, A.; Ustinov, A. Diffraction patterns with m th order symmetry generated by sectional spiral phase plates. *J. Opt.* **2015**, *17*, 125607. [[CrossRef](#)]
28. Ruffato, G.; Massari, M.; Romanato, F. Generation of high-order Laguerre-Gaussian modes by means of spiral phase plates. *Opt. Lett.* **2014**, *39*, 5094–5097. [[CrossRef](#)]
29. Masajada, J. Half-plane diffraction in the case of Gaussian beams containing an optical vortex. *Opt. Commun.* **2000**, *175*, 289–294. [[CrossRef](#)]
30. Bekshaev, A.; Chernykh, A.; Khoroshun, A.; Mikhaylovskaya, L. Localization and migration of phase singularities in the edge-diffracted optical-vortex beams. *J. Opt.* **2016**, *18*, 024011. [[CrossRef](#)]
31. Masajada, J.; Leniec, M.; Drobczyński, S.; Thienpont, H.; Kress, B. Micro-step localization using double charge optical vortex interferometer. *Opt. Express* **2009**, *17*, 16144–16159. [[CrossRef](#)]
32. Spektor, B.; Normatov, A.; Shamir, J. Singular beam microscopy. *Appl. Opt.* **2008**, *47*, A78–A87. [[CrossRef](#)]
33. Masajada, J.; Leniec, M.; Jankowska, E.; Thienpont, H.; Ottevaere, H.; Gomez, V. Deep microstructure topography characterization with optical vortex interferometer. *Opt. Express* **2008**, *16*, 19179–19191. [[CrossRef](#)] [[PubMed](#)]
34. Anzolin, G.; Tamburini, F.; Bianchini, A.; Barbieri, C. Method to measure off-axis displacements based on the analysis of the intensity distribution of a vortex beam. *Phys. Rev. A* **2009**, *79*, 033845. [[CrossRef](#)]
35. Singh, R.K.; Senthilkumaran, P.; Singh, K. Tight focusing of vortex beams in presence of primary astigmatism. *J. Opt. Soc. Am. A* **2009**, *26*, 576–588. [[CrossRef](#)] [[PubMed](#)]
36. Singh, R.K.; Senthilkumaran, P.; Singh, K. Structure of a tightly focused vortex beam in the presence of primary coma. *Opt. Commun.* **2009**, *282*, 1501–1510. [[CrossRef](#)]
37. Masajada, J.; Leniec, M.; Augustyniak, I. Optical vortex scanning inside the Gaussian beam. *J. Opt.* **2011**, *13*, 035714. [[CrossRef](#)]
38. Dennis, M.R.; Götte, J.B. Topological aberration of optical vortex beams: Determining dielectric interfaces by optical singularity shifts. *Phys. Rev. Lett.* **2012**, *109*, 183903. [[CrossRef](#)]
39. Augustyniak, I.; Popiołek-Masajada, A.; Masajada, J.; Drobczyński, S. New scanning technique for the optical vortex microscope. *Appl. Opt.* **2012**, *51*, C117–C124. [[CrossRef](#)]
40. Popiołek-Masajada, A.; Sokolenko, B.; Augustyniak, I.; Masajada, J.; Khoroshun, A.; Bacia, M. Optical vortex scanning in an aperture limited system. *Opt. Lasers Eng.* **2014**, *55*, 105–112. [[CrossRef](#)]
41. Savelyev, D.A.; Khonina, S.N. Characteristics of sharp focusing of vortex Laguerre-Gaussian beams. *Comput. Opt.* **2015**, *39*, 654–662. [[CrossRef](#)]
42. Aksenov, V.P.; Pogutsa, C.E. The effect of optical vortex on random Laguerre-Gauss shifts of a laser beam propagating in a turbulent atmosphere. *Atmos. Ocean. Opt.* **2013**, *26*, 13–17. [[CrossRef](#)]
43. Morgan, K.; Miller, J.; Cochenour, B.; Li, W.; Li, Y.; Watkins, R.; Johnson, E. Free space propagation of concentric vortices through underwater turbid environments. *J. Opt.* **2016**, *18*, 104004. [[CrossRef](#)]
44. Soifer, V.A.; Korotkova, O.; Khonina, S.N.; Shchepakina, E.A. Vortex beams in turbulent media. *Komputernaja Opt.* **2016**, *40*, 605–624.
45. Rafayelyan, M.; Brasselet, E. Laguerre-Gaussian modal q-plates. *Opt. Lett.* **2017**, *42*, 1966–1969. [[CrossRef](#)] [[PubMed](#)]
46. Stamnes, J.J. *Waves in Focal Regions: Propagation, Diffraction and Focusing of Light, Sound and Water Waves*; Routledge: Abingdon, UK, 2017.
47. Kotlyar, V.V.; Kovalev, A.A.; Porfirev, A.P. Elliptic Gaussian optical vortices. *Phys. Rev. A* **2017**, *95*, 053805. [[CrossRef](#)]
48. Rumi, G.; Actis, D.; Amaya, D.; Gomez, J.; Rueda, E.; Lencina, A. Analytical description of optical vortex beams generated by discretized vortex producing lenses. *arXiv Preprint* **2017**, arXiv:1711.06911.

49. Berry, M. Optical vortices evolving from helicoidal integer and fractional phase steps. *J. Opt. A Pure Appl. Opt.* **2004**, *6*, 259. [[CrossRef](#)]
50. Bekshaev, A.Y.; Karamoch, A. Displacements and deformations of a vortex light beam produced by the diffraction grating with embedded phase singularity. *Opt. Commun.* **2008**, *281*, 3597–3610. [[CrossRef](#)]
51. Bekshaev, A.Y.; Sviridova, S. Effects of misalignments in the optical vortex transformation performed by holograms with embedded phase singularity. *Opt. Commun.* **2010**, *283*, 4866–4876. [[CrossRef](#)]
52. Płociniczak, Ł.; Popiołek-Masajada, A.; Masajada, J.; Szatkowski, M. Analytical model of the optical vortex microscope. *Appl. Opt.* **2016**, *55*, B20–B27. [[CrossRef](#)]
53. Płociniczak, Ł.; Popiołek-Masajada, A.; Szatkowski, M.; Wojnowski, D. Transformation of the vortex beam in the optical vortex scanning microscope. *Opt. Laser Technol.* **2016**, *81*, 127–136.
54. Kotlyar, V.; Kovalev, A. Family of hypergeometric laser beams. *J. Opt. Soc. Am. A* **2008**, *25*, 262–270. [[CrossRef](#)] [[PubMed](#)]
55. Kotlyar, V.; Kovalev, A.; Porfirev, A. Asymmetric Gaussian optical vortex. *Opt. Lett.* **2017**, *42*, 139–142. [[CrossRef](#)] [[PubMed](#)]
56. Mair, A.; Vaziri, A.; Weihs, G.; Zeilinger, A. Entanglement of the orbital angular momentum states of photons. *Nature* **2001**, *412*, 313–316. [[CrossRef](#)] [[PubMed](#)]
57. Chen, Q.F.; Shi, B.S.; Zhang, Y.S.; Guo, G.C. Entanglement of the orbital angular momentum states of the photon pairs generated in a hot atomic ensemble. *Phys. Rev. A* **2008**, *78*, 053810. [[CrossRef](#)]
58. Popiołek-Masajada, A.; Masajada, J.; Kurzynowski, P. Analytical model of the optical vortex scanning microscope with a simple phase object. *Photonics* **2017**, *4*, 38. [[CrossRef](#)]
59. Popiołek-Masajada, A.; Masajada, J.; Lamperska, W. Phase recovery with the optical vortex microscope. *Meas. Sci. Technol.* **2019**, *30*, 105202. [[CrossRef](#)]
60. Goodman, J.W. *Introduction to Fourier Optics*; Roberts and Company Publishers: Greenwood Village, CO, USA, 2005.
61. Abramowitz, M.; Stegun, I.A. *Handbook of Mathematical Functions with Formulas, Graphs, and Mathematical Tables*, 9th ed.; Dover Publications: Mineola, NY, USA, 1972; Chapter: Confluent Hypergeometric Functions, pp. 503–515.
62. Nye, J.F. *Natural Focusing and Fine Structure of Light: Caustics and Wave Dislocations*; CRC Press: Boca Raton, FL, USA, 1999.
63. Ricci, F.; Löffler, W.; Van Exter, M. Instability of higher-order optical vortices analyzed with a multi-pinhole interferometer. *Opt. Express* **2012**, *20*, 22961–22975. [[CrossRef](#)]
64. Neo, R.; Tan, S.J.; Zambrana-Puyalto, X.; Leon-Saval, S.; Bland-Hawthorn, J.; Molina-Terriza, G. Correcting vortex splitting in higher order vortex beams. *Opt. Express* **2014**, *22*, 9920–9931. [[CrossRef](#)]
65. Zambrana-Puyalto, X.; Vidal, X.; Fernandez-Corbaton, I.; Molina-Terriza, G. Far-field measurements of vortex beams interacting with nanoholes. *Sci. Rep.* **2016**, *6*, 1–10. [[CrossRef](#)]
66. Ferrando, A.; García-March, M. Analytical solution for multi-singular vortex Gaussian beams: The mathematical theory of scattering modes. *J. Opt.* **2016**, *18*, 064006. [[CrossRef](#)]
67. Gibson, G.; Courtial, J.; Padgett, M.J.; Vasnetsov, M.; Pas'ko, V.; Barnett, S.M.; Franke-Arnold, S. Free-space information transfer using light beams carrying orbital angular momentum. *Opt. Express* **2004**, *12*, 5448–5456. [[CrossRef](#)] [[PubMed](#)]

